reinforcement at mid-span decreased, which is expected since more load is required to produce the same mid-span strain as flexural reinforcement ratio increases. The beams without stirrups all failed in shear-tension. The cracks ran from the load plate to the bearing plate for BM12-INF and BM16-INF, and from the load plate to the quarter span for BM25-INF. Splitting cracks formed on the sides of the beams following peak load. Figure 3 shows a photo at the point of peak load for BM12-INF and BM25-INF.

Beams with stirrups all failed in a form of shear-compression. The failure loads and maximum deflections were not dependant on the amount and placement of flexural reinforcement, since the primary failure mechanism was the crushing of the web concrete confined by the stirrups. Peak load was not accompanied by loud noises, movement, or the spitting of concrete projectiles, but infrequent slight popping noises consistent with sound of concrete fracture could be heard in the vicinity of peak load. Generally, these beams displayed some degree of post peak ductility. Cracking in these beams was typical: the mid-span flexural crack formed first, followed by others at the location of stirrups which transformed into flexural-shear cracks before the formation of shear cracks. The failure planes and critical shear cracks ran from the load plate to the bearing plate. Figure 4 shows a photo at the point of peak load for BM12-220 and BM25-220.

Figure 5 shows the load-displacement plots for the beams. Small discontinuities in the curves may show either the formation and growth of cracks or occasions where loading was stopped for crack width measurements. The load-displacement plots show that the beams with the larger flexural reinforcement ratios had stiffer load-displacement responses. The plot also shows that beams with stirrups showed some degree of post-peak ductility as a result of the concrete confinement provided by the stirrups.

Figure 6 shows plots of load against mid-span strain in the outermost layer of flexural reinforcement. The mid-span readings for beams BM12-220 and BM16-220 stop abruptly within the vicinity of peak load due to gauge failures. The reinforcement strains show a very stiff initial strain response until the mid-span flexural crack formed, at which point the response softened. Readings then conformed to linear elastic behaviour until peak load. Figure 7 is a plot of the load against stirrup strain for beam BM12-220, and is typical of all beams with stirrups. The labels A & B in Figure 7 refer to the stirrups identified were Figure 8. In all beams with stirrups, only the gauges on the straight portion of a stirrup leg were significantly engaged.

The beams with stirrups failed in shear-compression with critical shear cracks and compression struts that ran from load plate to each support plate. Failure occurred by concrete crushing in the upper portion of the beam along one of the critical shear cracks. For beam BM12-220, shown in Figures 7 & 8, the failure plane was on the opposite shear span from that pictured; the pictured shear span shows the instrumented one. The critical shear crack in Figure 8 crosses the two instrumented stirrups near mid-height of the stirrup leg, close to the gauges attached to the straight portion of the stirrups. The engagement of the stirrups does not occur until the formation of flexural-shear cracks at approximately 150 kN (33.7 kip), which is indicated by the gauges on the straight portion. The stirrup bend gauges do not show strain until a load of approximately 200 kN (45.0 kip), a point after the establishment of critical shear cracks, which formed at approximately 175 kN (39.3 kip). These results suggest that GFRP stirrup bend strength may not be a critical factor in the failure of deep beams.

To confirm that no stirrups ruptured, a select few were extracted from beams using a jackhammer and hacksaw. The bend of one such stirrup is shown in Figure 9, and was taken from the failed shear span of beam BM12-220. It is clear that the stirrup has not failed; however, this flexural-tension zone bend shows distress in the form of a crack. The crack runs through the bend in a plane perpendicular to the plane of the stirrup along what could be considered the central axis of the bar.

THE INDETERMINATE STRUT-AND-TIE (IST) METHOD

The IST method is an adaptation of work by Kim and Yun (2011a, b). In the first paper, they use their method to determine the point of "balanced shear failure" in steel reinforced deep beams, a point defined by the simultaneous yielding of stirrups and crushing of the direct-strut. In the same paper, they then developed an equation to predict the load distribution ratio for the direct-strut and stirrup-truss load paths, turning an indeterminate strut-and-tie design into two separate determinate designs. In the second paper (2011b), they show that their load distribution ratio equation leads to good strength predictions using a large experimental dataset.

Kim and Yun's (2011a) method for determining the point of balanced shear failure was adapted for use with FRP reinforced deep beams. The indeterminate strut-and-tie method is a stress field method using truss elements and incorporating one-dimensional concrete non-linearity. It can be applied to situations, such as the analysis of a reinforced concrete deep beam, where the stress field behaviour is governed by the changing stiffnesses of the truss elements. In the case of FRP reinforced concrete, the FRP reinforcement remains linear elastic while the concrete struts soften as load increases. The strength of concrete strut elements is reduced using a softening coefficient applied to the peak load and strain at peak load parameters of the concrete material model, as done by Kim and Yun (2011a). Further adaptations for FRP reinforcement included modifications to the reinforcement material behaviour and changes to the methodology by which the geometry of struts and nodal zones are defined. Details of the method and an example analysis may be found in (Krall, 2014).

The IST method is a stiffness based method; load is applied incrementally and the global stiffness matrix is updated to account for changing strut elasticity on each iteration. Concrete elasticity is defined by the tangent modulus, and the crushing of a strut is defined by the point of peak load – where the elasticity is zero. The highest possible failure load occurs when the model becomes unstable as a result of failures in the individual elements; though judgement is required to determine if the failure of individual elements at a lower load may result in beam failure in the event of overlapping struts or premature nodal failure, for example.

The IST method has only been used to model the GFRP reinforced deep beams from the research programme in (Krall, 2014), but is defined generally enough that it could be applied to other concrete D-regions.

RESULTS OF THE ANALYSIS

The results from the experimental programme were compared to the predictions of the IST method, the ACI 440.1R-06 guidelines, the CSA S806-12 standard, and a model from literature (Nehdi et al. 2007). The "optimized equations" model from Nehdi et al. (2007), their equations 3 & 4, were used. Nehdi et al. (2007) also developed a set of "design equations" by modifying the coefficients of the optimized equations to make them more conservative. Machial et al. (2012) found the design equations to be one of the best predictors of shear strength when compared to eight other models. The optimized equations were used in this research programme as they are more relevant to an academic investigation where factors for conservatism are often discarded.

The IST method trusses used in the analysis are shown in Figure 10, where symmetry allowed for the modelling of half the beam. The truss for beams without stirrups is determinate, beams BMX-INF in Figure 10. This truss had one strut called the direct-strut and one tension tie representing the flexural reinforcement. The model for beams with stirrups placed a tie at the location of each stirrup, beams BMX-220 in Figure 10. This truss model did not include the left most stirrup, shown in Figure 1, as this stirrup did not engage during the tests (Krall, 2014). This truss is indeterminate and is composed of two load paths, or mechanisms. The first is the direct-strut mechanism which is the load path described for the beams without stirrups, see BMX-INF in Figure 10. The second is the stirrup-truss mechanism, which includes the stirrup-ties, top chord struts, and the remaining diagonal struts. Both mechanisms share the same flexural reinforcement tie. The vertical tie at mid-span is a zero force member, but is included for completeness (Krall, 2014).

The results and predictions are presented in Table 4. The material parameters used in the analysis are those described above in the Material Properties section. The inputs into the IST method include all parameters required to solve a truss system, such as element geometry and boundary conditions, in addition to material models, such as the softening coefficient modified Hognestad Parabola as described by Kim and Yun(2011a), (Krall, 2014). The term V_E and V_P refer to the experimental and predicted shear strength, respectively.

The IST method made very good predictions for all beams, having the closest prediction of shear strength for four of the six beams. The IST method has the best average, and the individual predictions from the IST method vary from the mean the least of the four models presented. The Nehdi et al. (2007) model also made good predictions, outperforming the two design models.

There are two very notable features in Table 4. First, the CSA S806-12 standard significantly over-predicts the shear strength of deep beams without stirrups, beams BMX-INF; the use of material factors of safety as per the CSA

S806-12 standard would not make the predictions conservative. Otherwise, CSA S806-12 standard under-predicts the strength of beams with stirrups. Second, the ACI 440.1R-06 guidelines significantly under-predict the shear strength of GFRP reinforced deep beams both with and without stirrups, which conforms to the findings of the investigation of Machial et al. (2012).

The poor performance of the two design standard models in predicting the shear strength of the beams with stirrups is not unexpected. Both were sectional shear models, which are not formulated for use with deep beams. The predictions from these models were conservative, because sectional shear models do not account for the increased load carrying capacity resulting from arch action.

The IST method and Nehdi et al. (2007) optimized equations performed better because they were both formulated for use with deep beams. The IST method is a strut-and-tie method and is thus specifically intended for the analysis of D-regions, such as deep beams. The Nehdi et al. (2007) set of optimized equations was derived using genetic algorithm programing, a very sophisticated form of curve fitting, on a database that included both slender and deep beams.

CONCLUSIONS

The results of an experimental investigation done on concrete beams reinforced with GFRP in both flexure and shear are discussed in this paper. A novel strut-and-tie method, known as the indeterminate strut-and-tie method, was adapted from the work of Kim & Yun (2011a) and introduced for the analysis experiments.

The experimental portion of the research programme found that beams without stirrups failed in shear-tension, while beams with stirrups showed deep beam behaviour and failed in shear-compression. The beams without stirrups showed very little post-peak ductility, whereas the beams with stirrups showed some ductility. Mid-span strain results indicated linear elastic behaviour, as expected. Beams with larger flexural reinforcement ratios showed stiffer load-displacement responses.

No stirrups ruptured during the tests but an inspection of extracted stirrups found signs of distress along the central axis of a stirrup bar in the flexural-tension zone bend.

The stirrup strain readings indicated that the flexural-tension zone bends of the stirrups never experienced appreciable elongation; however, significant strain was recorded by gauges on the straight portion of the stirrup legs at mid-height of the beams. The critical shear crack ran from the load plates to the bearing plates and generally crossed the instrumented stirrups where the straight portion gauges were located.

The results were compared to predictions made by four shear strength models: The IST method, the ACI 440.1R-06 model, CSA S806-12 model, and the Nehdi et al. (2007) optimized equations. The IST method and the Nehdi et al. model were very good at predicting beam strength, since they were both intended for use with deep beams. The IST method had a better experimental-to-predicted strength ratio overall for the tested beams, and the least variability amongst the methods. The ACI model significantly under-predicted shear strength, while the CSA model dangerously over-predicted the strength of beams without stirrups, but otherwise also under-predicted the strength of beams with stirrups.

ACKNOWLEDGEMENTS

The authors would like to express their gratitude and appreciation to Schoeck Canada and HOGG Ready Mix for their donations to the research programme. The authors would also like to thank the structural laboratory technical staff as well as the graduate students at the University of Waterloo who helped with specimen fabrication and testing.

REFERENCES

Ahmed, E. A., El-Sayed, A. K., El-Salakawy, E. F., Benmokrane, B., "Bend Strength of FRP Stirrups: Comparison and Evaluation of Testing Methods", *Journal of Composites for Construction*, 14(1), (February) 2010, pp 3-10.

American Concrete Institute (ACI), "Guide for the Design and Construction of Structural Concrete Reinforced with FRP Bars (ACI 440.1R-06)", American Concrete Institute, Farmington Hills, Michigan, 2006.

Andermatt, M. F., Lubell, A. S., "Strength Modeling of Concrete Deep Beams Reinforced with Internal Fiber-Reinforced Polymer", *ACI Structural Journal*, 110(4), (July-August) 2013, pp 595-606.

Canadian Standards Association (CSA), "Design and Construction of Building Structures with Fibre-Reinforced Polymers (CAN/CSA S806-12)", Canadian Standards Association, Mississauga, Ontario, Canada, March 2012.

Farghaly, A. S., Benmokrane, B., "Shear Behaviour of FRP-Reinforced Concrete Deep Beams without Web Reinforcement", *Journal of Composites for Construction*, 17(6), (December) 2013, pp N/A.

Imjai, T., Guadagnini, M., Pilakoutas, K., "Mechanical Performance of Curved FRP Rebars - Part I: Experimental Study", *Proceedings of the First Asia-Pacific Conference on FRP in Structures, APFIS 2007, by the International Institute for FRP in Construction (IIFC)*, Hong Kong, China, (December) 2007, Ed. Smith S. T., University of Hong Kong, Hong Kong, China, pp 333-338.

Kanematsu, H., Sato, Y., Ueda, T., Kakuta, Y., "A Study on Failure Criteria of FRP Rods Subject to Tensile and Shear Force", *Proceedings of FIP Symposium '93 "Modern Prestressing Techniques and Their Applications"*, Kyoto, Japan, (October) 1993, Japan Prestressed Concrete Engineering Association, pp 743-750.

Kim, B. H., Yun, Y. M, "An Indeterminate Strut-Tie Model and Load Distribution Ratio for RC Deep Beams – (I) Model & Load Distribution Ratio", *Advances in Structural Engineering*, 14(6), (December) 2011a, pp 1031-1041.

Kim, B. H., Yun, Y. M, "An Indeterminate Strut-Tie Model and Load Distribution Ratio for RC Deep Beams – (II) Validity Evaluation", *Advances in Structural Engineering*, 14(6), (December) 2011b, pp 1043-1057.

Krall, M. D., "Tests on Concrete Beams with GFRP Flexural and Shear Reinforcements & Analysis Method for Indeterminate Strut-and-Tie Models with Brittle Reinforcements", Master's Thesis, Department of Civil and Environmental Engineering, University of Waterloo, Waterloo, Ontario, Canada, 2014.

Machial, R., Shahria Alam, M., Rteil, A., "Revisiting the Shear Design Equations for Concrete Beams Reinforced with FRP Rebar and Stirrup", *Materials and Structures*, 45(11), (November) 2012, pp 1593-1612.

Nehdi, M., El Chabib, H., Aly Said, A., "Proposed Shear Design Equations for FRP-Reinforced Concrete Beams Based on Genetic Algorithms Approach", *Journal of Materials in Civil Engineering*, 19(12), (December) 2007, pp 1033-1042.

Schoeck Canada Inc., "Schöck ComBAR Technical Information (Doc ID: WK0437/03.3011/CA/110119)", Schoeck Canada Inc., Kitchener, Ontario, Canada, March 2011.

Shehata, E., Morphy, R., Rizkalla, S., "Fibre Reinforced Polymer Shear Reinforcement for Concrete Members: Behaviour and Design Guidelines", *Canadian Journal of Civil Engineering*, 27(5), (October) 2000, pp 859-872.

Yun, Y. M., Ramirez, J. A., "Strength of Struts and Nodes in Strut-Tie Model", *Journal of Structural Engineering*, 122(1), (January) 1996, pp 20-29.

Yun, Y. M., "Nonlinear Strut-Tie Model approach for Structural Concrete", *ACI Structural Journal*, 97(4), (July-August) 2000, pp 581-590.

Yun, Y. M, Kim, B. H., "Two-Dimensional Grid Strut-Tie Model Approach for Structural Concrete", *Journal of Structural Engineering*, 134(7), (July) 2008, pp 1199-1214.

Table 1—As-Designed Parameters

Beam	**Units**	**BM25-INF/220**	**BM16-INF/220**	**BM12-INF/220**
Height, *h*	**mm**	330	345	350
	(inch)	(12.99)	(13.58)	(13.78)
Length, *l*	**mm**	2470	1930	1810
	(inch)	(97.24)	(75.98)	(71.26)
Total FRP Area, A_{frp}	**mm**	982	1206	1356
	(inch)	(1.52)	(1.87)	(2.10)
ρ	**%**	1.82	2.23	2.51

Table 2—GFRP Properties (Schoeck Canada Inc., 2011)

Property	**Units**	**Ø25**	**Ø16**	**Ø12**	**Ø12 Stirrup**
Straight Portion Strength, $f_{u\_straight}$	**MPa**	1000	1000	1000	1000
	(ksi)	(145)	(145)	(145)	(145)
Bent Portion Strength, f_{u_bent}	**MPa**	-	-	-	700
	(ksi)				(102)
Modulus of Elasticity, E_f	**GPa**	60	64	60	50
	(ksi)	(8702)	(9282)	(8702)	(7252)
Rupture Strain, ε_{Fu}	**%**	-	2.61	-	-

Table 3—Summary of Experimental Results

Beam	ρ_f	P_E		Δ_{mid} **at** P_E		**Longitudinal** ε_{max}	**Stirrup Bend** ε_{max}	**Stirrup Straight** ε_{max}
	%	**kN**	**(kip)**	**mm**	**(inch)**	**με**	**με**	**με**
BM12-INF	2.5	163.1	(36.67)	4.25	(0.167)	2523	-	-
BM16-INF	2.2	150.2	(33.77)	4.21	(0.166)	2744	-	-
BM25-INF	1.8	125.1	(28.12)	3.22	(0.127)	2919	-	-
BM12-220	2.5	382.4	(85.97)	11.96	(0.471)	*7448*	*1237*	*4952*
BM16-220*	*2.2*	*309.3*	*(69.53)*	*8.42*	*(0.331)*	*5863*	*256*	*4742*
BM25-220	1.8	360.1	(80.95)	24.01	(0.945)	8783	11484	*10558*

**BM16-220 experienced one unintended 43% load cycle before failure.*

Table 4—Comparison of Experimental and Predicted Strengths

		ACI 440.1R-06		**CSA S806-12**		**Nehdi et al.**†		**IST Method**	
Beam	V_E*	V_P*	V_E/V_P	V_P*	V_E/V_P	V_P*	V_E/V_P	V_P*	V_E/V_P
	kN/(kip)	**kN/(kip)**		**kN/(kip)**		**kN/(kip)**		**kN/(kip)**	
BM12-INF	81.5 (18.3)	38.8 (8.7)	2.10	121.9 (27.4)	0.67	72.4 (16.3)	1.13	72.7 (16.3)	1.12
BM16-INF	75.1 (16.9)	37.9 (8.5)	1.98	117.9 (26.5)	0.64	71.6 (16.1)	1.05	70.5 (15.8)	1.07
BM25-INF	62.6 (14.1)	33.8 (7.6)	1.85	114.9 (25.8)	0.54	67.3 (15.1)	0.93	66.7 (15.0)	0.94
BM12-220	191.2 (43.0)	94.3 (21.2)	2.03	146.2 (32.9)	1.31	164.5 (37.0)	1.16	195.5 (44.0)	0.98
BM16-220*	*154.6 (34.8)*	*93.4 (21.0)*	*1.65*	*141.2 (31.7)*	*1.10*	*163.7 (36.8)*	*0.94*	*197.5 (44.4)*	*0.78*
BM25-220	180.0 (40.5)	89.3 (20.1)	2.02	134.3 (30.2)	1.34	159.4 (35.8)	1.13	197.1 (44.3)	0.91
Average =**			2.00		0.90		1.08		1.00

†*Equations 3 & 4 from Nehdi et al. (2007).*
**V = 0.5P, where V is shear and P is applied load.*
***Outlier not included in averages.*

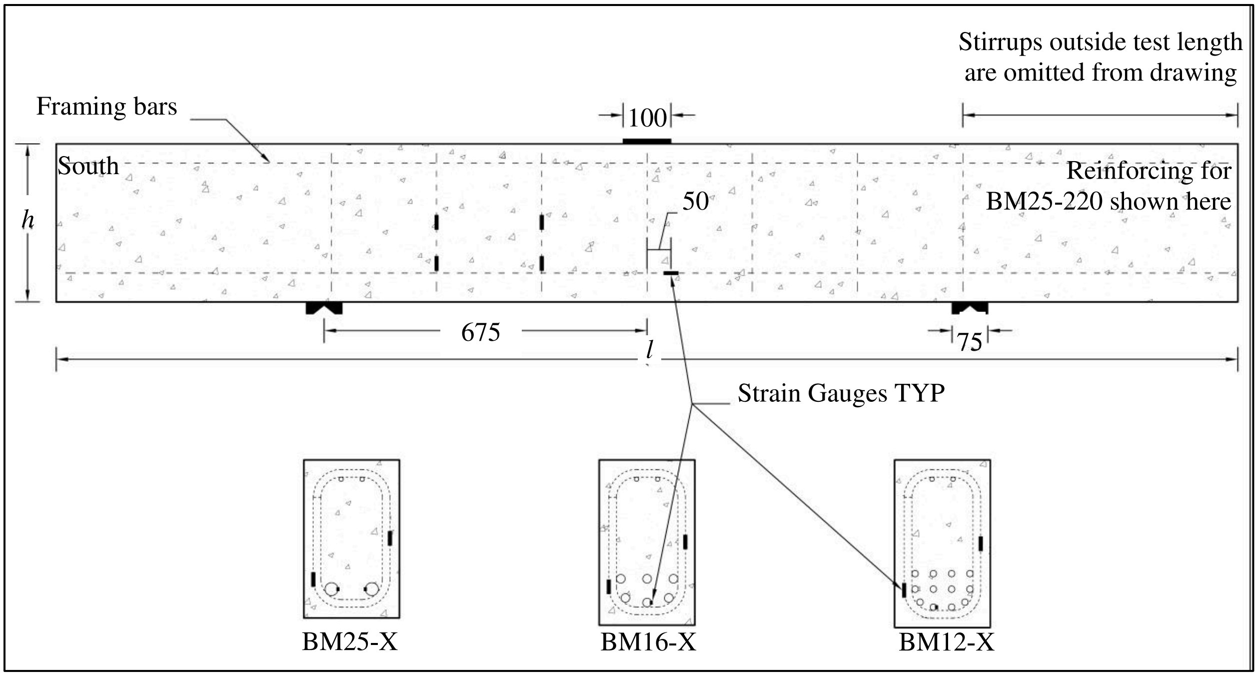

Figure 1—Elevation of BM25-220 and Cross-Sections

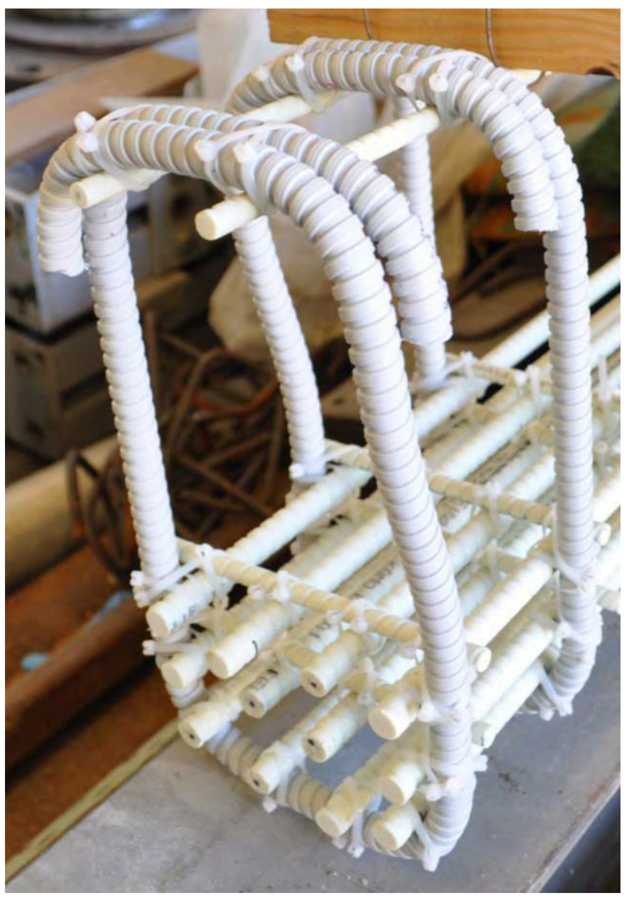

Figure 2—Image of GFRP Reinforcement

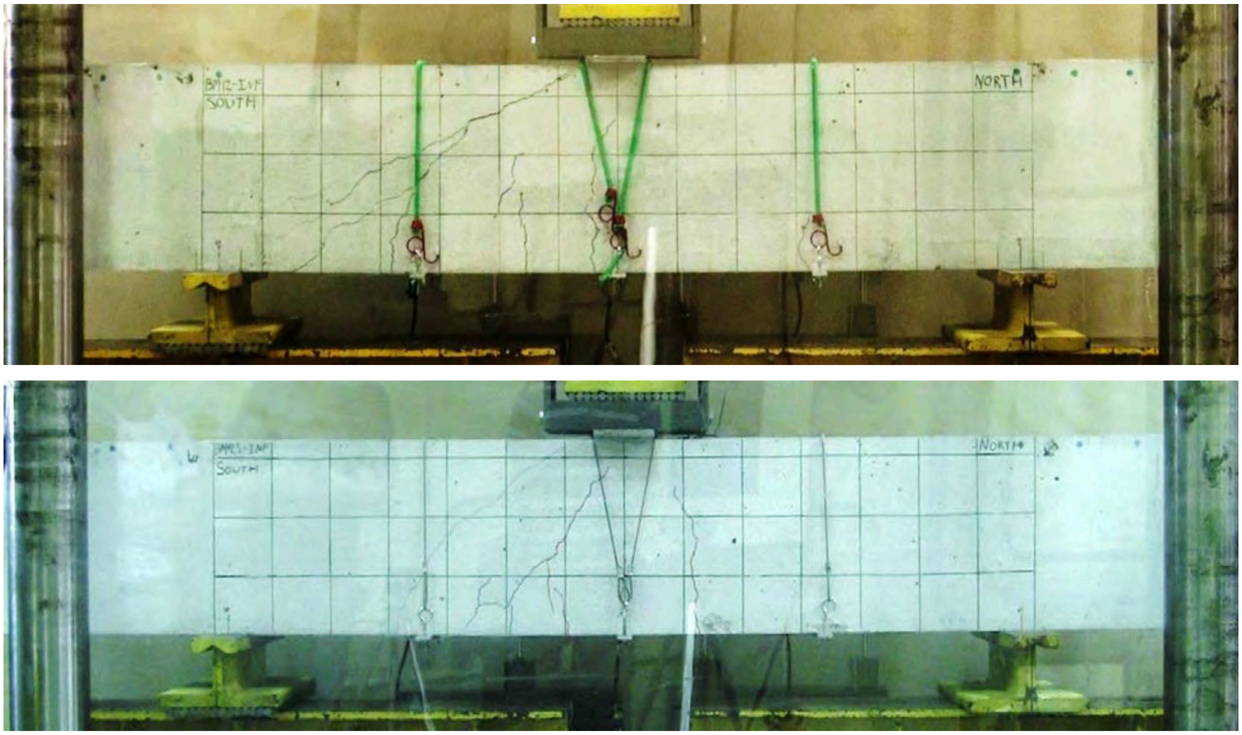

Figure 3—BM12-INF (above) and BM25-INF (below) at Peak Load

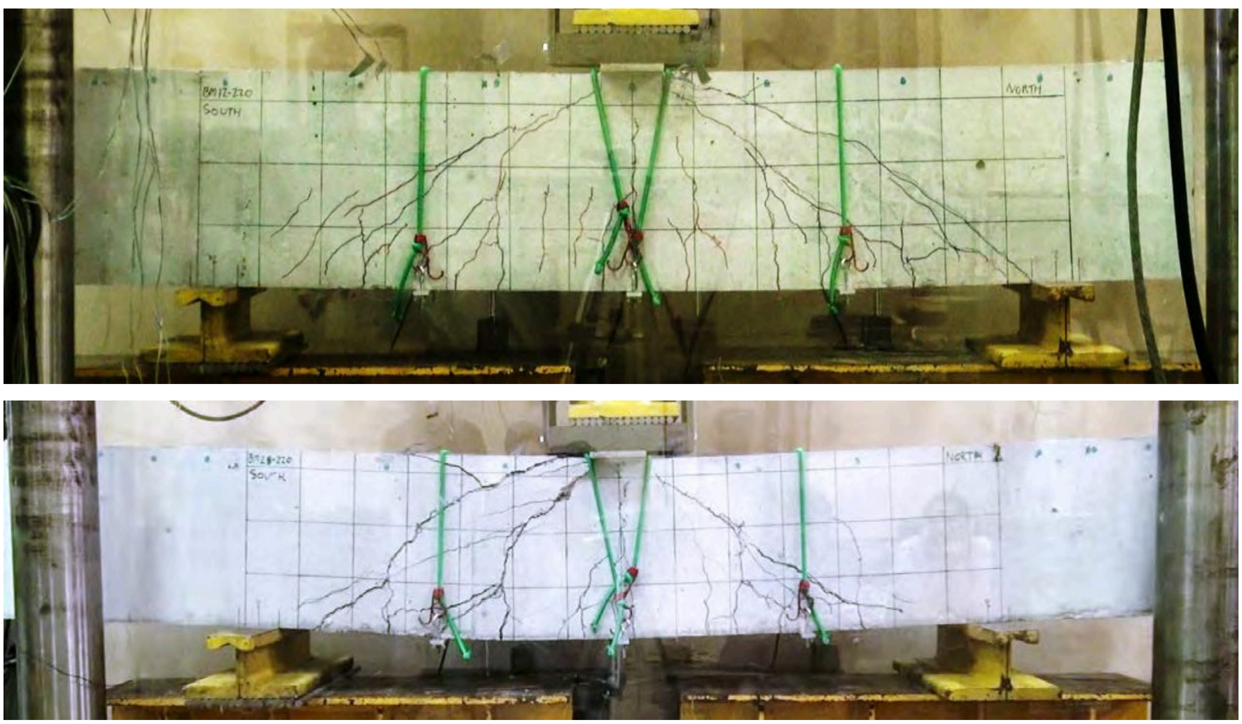

Figure 4—BM12-220 (above) and BM25-220 (below) at Peak Load

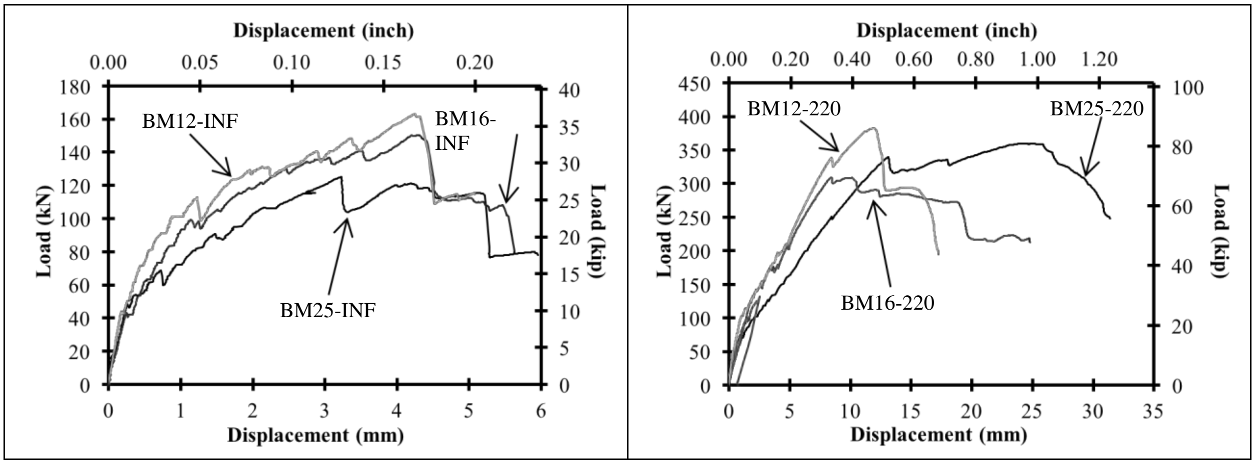

Figure 5—Load vs Displacement Curves for All Specimens

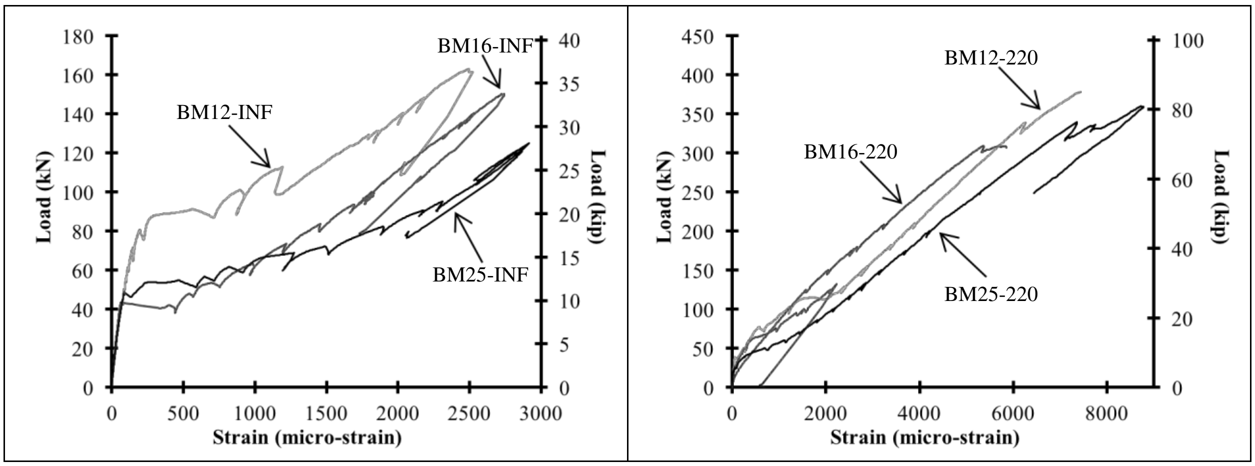

Figure 6—Load vs Mid-span Strain Curves for All Specimens

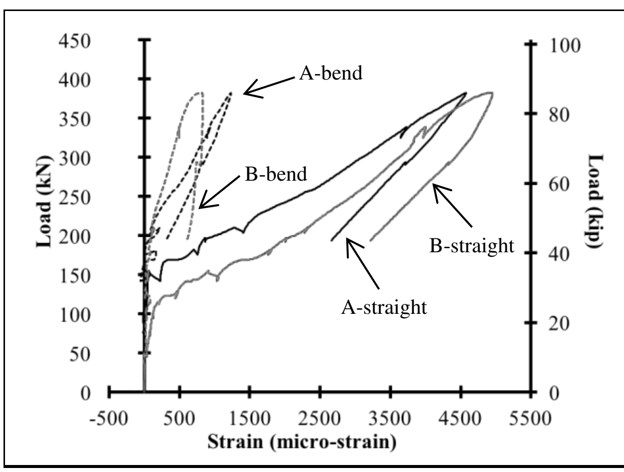

Figure 7—Load vs Stirrup Strain for BM12-220

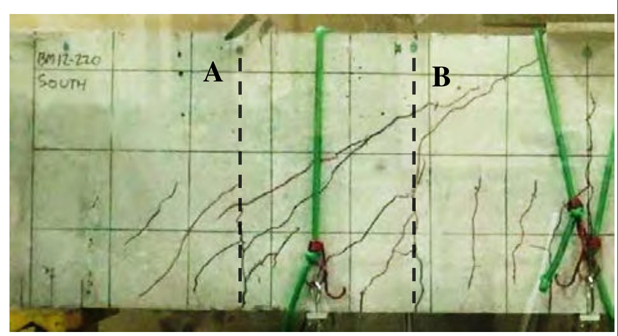

Figure 8—Crack Diagram for BM12-220 at Peak Load

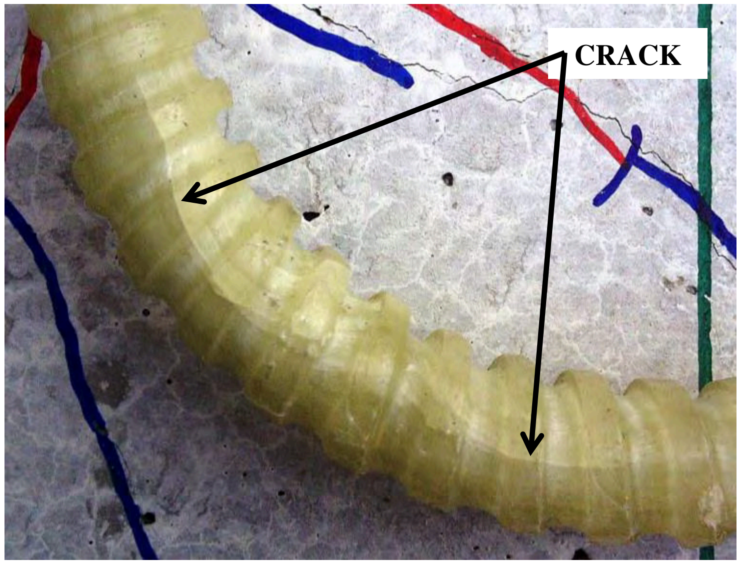

Figure 9—Retrieved Stirrup with Crack from BM12-220 (Krall, 2014)

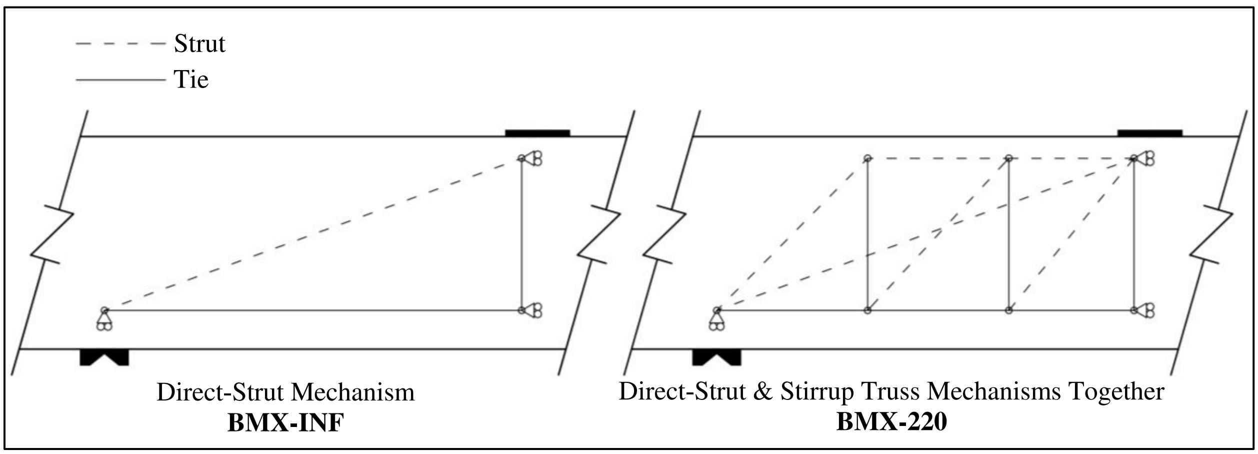

Figure 10—IST Method Trusses

Hollow-Core FRP-Concrete-Steel Tubular Columns Subjected to Seismic Loading

Omar I. Abdelkarim, Ahmed Gheni, Sujith Anumolu, and Mohamed A. ElGawady

Synopsis: This paper describes the behavior of precast hollow-core fiber-reinforced polymer (FRP)-concrete-steel columns (HC-FCS) under combined axial and lateral loading. The HC-FCS column consists of a concrete wall sandwiched between an inner steel tube and an outer FRP tube. This study investigated two large-scale columns: the traditional reinforced concrete (RC) and the HC-FCS column. The steel tube of the HC-FCS column was embedded into the footing while the FRP tube was stopped at the top of the footing level (i.e., the FRP tube provided confinement only). The hollow steel tube provided the only reinforcement for shear and flexure inside the HC-FCS column. The FRP in HC-FCS ruptured at a lateral drift of 15.2%, while the RC column displayed a 10.9% lateral drift at failure. The RC column failed due to rebar rupture when the moment capacity dropped more than 20%. The HC-FCS failed gradually with concrete compression failure and steel local buckling followed by FRP rupture. Finite element (FE) analysis was conducted using LS-DYNA to develop a static cyclic analysis of a three-dimensional HC-FCS model. The FE results mirrored the experimental results. The bending strength of HC-FCS columns could easily be calculated with a high degree of accuracy using a sectional analysis based on Navier-Bernoulli's assumptions and strain compatibility concepts.

Keywords: Bridge columns; precast columns; composite columns; hollow columns; seismic loading